Selective epitaxy of semiconductor nanopyramids for nanophotonics
Poole, P. J.; Dalacu, D.; Lefebvre, J.; Williams, R. L.

National Research Council Canada   Conseil national de recherches Canada

Canada

Selective epitaxy of semiconductor nanopyramids for nanophotonics

Selective epitaxy of semiconductor nanopyramids for nanophotonics

P J Poole, D Dalacu, J Lefebvre and R L Williams

Institute for Microstructural Sciences, National Research Council, Ottawa, ON, K1A 0R6,
Canada

E-mail: philip.poole@nrc-cnrc.gc.ca

Abstract
We present a detailed study of the parameters which affect the geometrical perfection of
nanopyramids used for the site-selected nucleation of quantum dots. Through an understanding
of crystal facet formation, we demonstrate that undesirable high index planes can be suppressed
using carefully optimized lithography together with properly oriented source fluxes in the
growth reactor. High quality InP nanopyramids are reported with individual InAs/InP quantum
dots positioned with high precision. This represents an important milestone for the fabrication
of complex quantum dot based nanophotonic devices.

1. Introduction

Nanostructures, such as self-assembled quantum dots (QDs) embedded in a semiconducting host by epitaxial growth, are very attractive for use as the active elements in optical and electronic devices relying on the properties of individual quantum states. For example, luminescent QDs can be used to create single photon sources [1, 2], entangled photon sources [3, 4] and quantum bits (qubits) for quantum computation [5]. Among several other parameters, the control of the position of these nanostructures is very important if they are to be used as the active elements in quantum devices. For example, the electronic states of a self-assembled QD only couple efficiently to an optical mode of a photonic crystal microcavity if the QD is accurately positioned within the antinode of the electric field profile corresponding to that optical mode [6]. Typical spatial full width at half maximum for the antinode is of the order of 200 nm, requiring positioning accuracy of better than ±50 nm. A number of approaches have been taken to provide this degree of position control which can be divided into two types; (1) the marking of the location of a randomly positioned QD and then fabricating the photonic crystal around it [7], and (2) the precise positioning of a single QD using a patterned growth process [8, 9]. The latter has the advantage of providing a scalable approach for the precise positioning of multiple single QDs. Without this ability the fabrication of more complex photonic devices, where multiple dots are coupled together, as required for example in an optical qubit, becomes very difficult, if not impossible. One successful example of a patterned growth process is the use of selective

area chemical beam epitaxy (CBE), demonstrated in our group, to form precisely positioned InP pyramids on which single InAs QDs are then grown [9, 10]. The approach of selective area epitaxy not only provides a high degree of positioning control, but has the added benefit of avoiding the introduction of other unwanted nearby emitters that could also couple to the cavity mode [11]. It is not enough to be able to reliably position a single QD, it must be of high optical quality and the growth highly reproducible. This is achieved by optimizing the growth of the pyramidal InP template, which has the benefit of separating the QD from the initial substrate/growth interface that typically accumulates impurities. The growth of a QD on this template depends on the facets that make up the template, so the growth behaviour of the InP pyramids has to be well understood. The purpose of this paper is to describe that growth behaviour and how it can be controlled to create optimal structures on which single InAs QDs can be grown.

2. Sample preparation

The structures in this study were all grown using chemical beam epitaxy (CBE) where the growth substrate has a patterned SiO_2 layer on the surface. This is prepared by depositing a 20 nm thick SiO_2 layer on a (001) InP substrate, e-beam patterning and then wet etching of the SiO_2 using a buffered HF etch. This results in openings in the SiO_2 surface exposing the InP substrate below. The source materials used for the InP growth were trimethylindium (TMI) as the source of indium, and precracked PH_3 (AsH_3) resulting predominantly in P_2 (As_2) as the phosphorus (arsenic) source. Growth was

performed at 515 °C using a planar growth rate of 0.05 nm s^{-1}. The use of an organometallic indium source, as opposed to the solid indium source used in molecular beam epitaxy, allows selective area epitaxy to be performed [12]. TMI landing on the SiO$_2$ surface will rapidly desorb from that surface, whilst any TMI that lands on the InP surface will crack, providing metallic indium for the growth of InP. This means that growth only occurs in the openings in the SiO$_2$ mask, and no deposition is observed on the SiO$_2$ itself. Selectivity is maintained over a wide range of growth conditions, from <400 to >550 °C. This selective behaviour is also observed for growth by metal-organic-chemical vapour-deposition (MOCVD), but unlike in MOCVD the low pressure growth conditions used for CBE means that there is no lateral transport of source materials across the SiO$_2$ mask, and hence no proximity effects to complicate mask design [12]. The growth in the openings of the mask results in facetted growth where the resulting facets are determined by the shape and orientation of the openings relative to the underlying crystal structure, and the growth conditions.

3. Results

3.1. Nanopyramid growth evolution

An easy way to determine which facets preferentially grow is to pattern a circular opening in the SiO$_2$ mask. The result of growth in such an opening is shown in figure 1(a), which is a (001) surface surrounded by eight well-defined low index facets. These facets are the four allowed {110} and {111} planes. The {111} planes can be further divided into sets of {111}A and {111}B planes since InP is a zinc-blende compound semiconductor. The A planes are indium terminated and the B planes are phosphorus terminated. The formation of the observed facetted structure is a consequence of breaking the crystal symmetry by confining the growth to a well-defined region, followed by different incorporation rates of indium on different facets combined with micron size diffusion lengths. As the growth initiates in the opening many different microfacets will form around the edge of the pattern. The ones that survive will be those for which the indium has a low incorporation rate, or equivalently a long incorporation length (the distance indium diffuses before incorporation into the lattice). Indium will move from facets with long incorporation lengths, in figure 1 the {110} and {111} facets, to ones with a lower incorporation length where it will preferentially incorporate, in this case the (001) facet, shown schematically in figure 1(b). This will hold true as long as the incorporation length on the {110} and {111} facets is significantly greater than the size of these facets. This results in an increase in the size of the side facets and a decrease of the top (001) surface. The final geometry of the structure will thus be dictated by these relative incorporation lengths, and will evolve through the sequential completion, and hence 'removal', of low incorporation length facets as demonstrated later.

The relative incorporation length of indium on different facets will depend on the growth conditions used, in particular
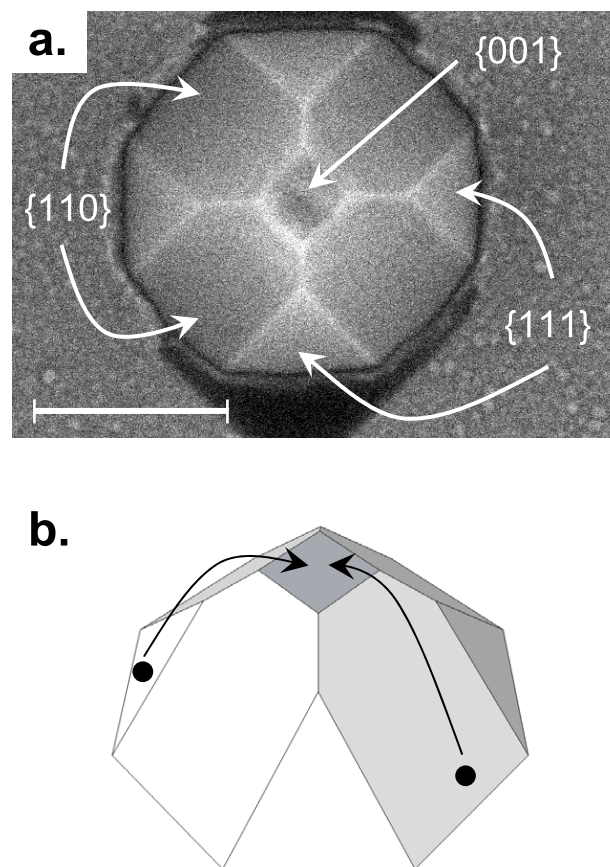

Figure 1. (a) Plan view SEM image of an InP pyramid selectively grown in a circular opening in a SiO$_2$ mask. The scale bar is 200 nm. (b) Schematic image of the pyramid.

growth temperature and V/III ratio [13–17]. In general the {110} facets are very smooth, while the {111} facets can be significantly rougher under some growth conditions. It is typically found that conditions favour one type of {111} facet (A or B) resulting in poor growth of the other.

Using the knowledge of the preferred facets, square openings were patterned in the SiO$_2$ mask with the sides of the square aligned in the ⟨100⟩ directions. To help understand the evolution of the pyramid formation a series of different size square openings were made. The result of this growth is shown in figure 2. Growth of a fixed amount of InP in different size square openings is geometrically equivalent to the growth of different amounts of InP in the same size opening. Thus going from the centre of the spiral (largest opening) outwards is geometrically equivalent to a time evolution of the growth of the InP pyramid structures. This holds true as long as the incorporation length of indium is greater than the size of the pyramids for all pyramids, as is the case here.

Figure 3 shows scaled images of four of the pyramids in figure 2. The images have been rescaled so that the initial square openings in the SiO$_2$ mask are the same size in all the images, as shown by the dashed square overlaid on top of each image. Beneath the SEM images are line drawings indicating the crystal structure for each of the pyramids. With the initial opening aligned in the ⟨100⟩ directions four {110} facets are
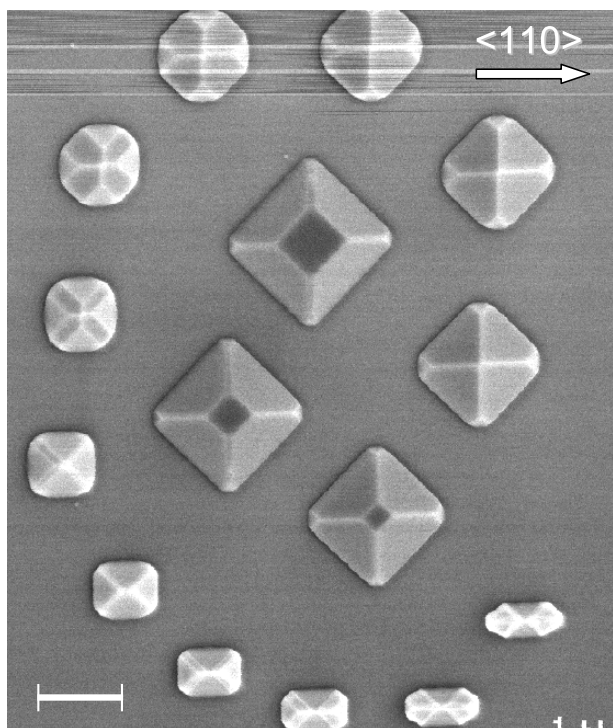
Figure 2. Plan view SEM image of InP pyramids selectively grown in different size square openings in the SiO$_2$ mask. All of the openings have their sides aligned in the ⟨100⟩ directions. The scale bar is 1 μm.
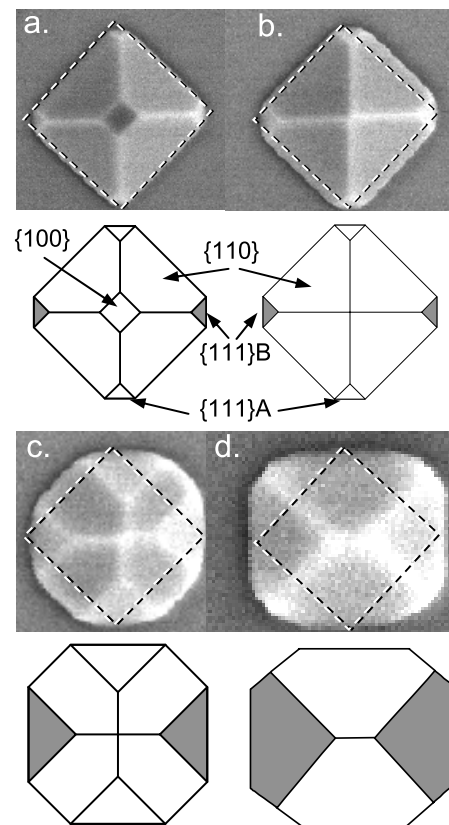

Figure 3. SEM images of four of the pyramids from figure 2 with progressively smaller openings, (a)–(d). The images have been rescaled so that the openings in the SiO$_2$ mask, indicated by the dashed squares, are the same size in all the images. Beneath each image is a schematic diagram of the corresponding pyramid. (a) Pyramid before completion of the (110) sidewalls. (b) Pyramid at the point of completion of the (110) sidewalls and the disappearance of the (001) top facet. (c) Pyramid after completion of the (110) sidewalls. Subsequent growth on the (110)s results in overgrowth of the SiO$_2$ mask and development of (111) facets. (d) Pyramid at the point of completion of the (111) sidewalls.

formed with the apex being the (001) surface. There is also evidence of small {111} facets at the base of the pyramid where the {110} facets meet, this is discussed in more detail later. As the growth progresses the pyramid grows taller through the incorporation of material only on the (001) facet with the material that lands on other facets diffusing to the (001) before incorporating. This results in a vertical growth rate for the (001) surface that is higher than observed for planar growth, and has to be taken into account if a specific pyramid height is required. This can be determined using geometric arguments similar to those used for the growth of ridges [18]. This continues until the pyramid completes to a point, figure 3(b), the (001) surface having been 'removed', or filled in.

Since there is no longer a (001) facet available, further growth requires the InP incorporation to occur on a different surface. The next most favourable facet for material incorporation is the {110} which grows exposing the small {111} facets in the bottom corners of the pyramids, figure 3(c). This requires the pyramid to grow over the SiO$_2$ surface, as can be clearly seen in figure 4. Growth on the {110} surfaces eventually results in their disappearance, as seen earlier for the (001) facet, resulting in a pyramid consisting only of {111} facets, figures 3(d) and 4. Thus the pyramid geometry evolves through the sequential completion, and hence 'removal', of low incorporation length facets. Since the {111}A and {111}B facets are chemically different, the A-face being In-terminated and the B-face P-terminated, if growth is continued it does so preferentially on the {111}A facets. Continued growth results in the formation of nanowires as described in [19]. The

growth of similar GaAs pyramidal structures have also been observed, where differences in the material system and growth conditions results in the preferential formation of a different sets of facets [20].

If the square openings in the SiO$_2$ mask are aligned to the ⟨110⟩ rather than the ⟨100⟩ directions then square based pyramids are also grown, but this time with {111} side facets and the usual top (001) surface. Growth will then progress as before through pyramid completion and then nanowire formation. We did not study these {111} pyramids further due to the enhanced As/P exchange that occurs on the {111}B sidewalls when growing the InAs QDs, as described later.

3.2. Dependence of growth on source flux orientation

In the growth of the common III–V semiconductors, such as GaAs and InP, by molecular beam epitaxy techniques such as CBE the growth rate is controlled by the supply of the group III species, with an excess of the volatile group V species provided to maintain stoichiometry. Changing group V flux
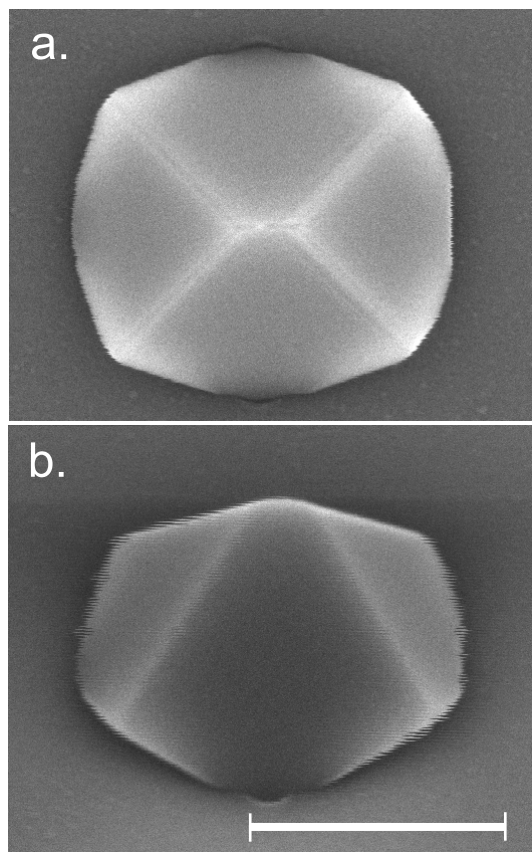
Figure 4. SEM images (a) plan view, and (b) at approximately 45°, of a structure grown to the point where it forms a completed {111} pyramid. The pyramid can be seen overgrowing the SiO$_2$ mask. The scale bar is 500 nm.

will typically modify the group III incorporation length [17], but this will have fairly subtle effects when growing on planar surfaces. It is a little more complicated when growing on structured surfaces, such as the pyramids [17, 21]. As described earlier, when the indium incorporation length is greater than the size of the pyramid the resulting facetted structure depends on the relative incorporation lengths on the different surfaces. This means that otherwise identical facets will grow in different ways if there is an asymmetry in the group V flux. This is demonstrated in figure 5 where pyramids are grown without substrate rotation, and for P$_2$ and TMI fluxes incident at different angles. Due to the geometry of the growth system the P$_2$ and TMI fluxes are always at a fixed angle of 17.5° relative to each other, and are changed relative to the sample normal by tilting and rotating the sample manipulator.

Figure 5(a) demonstrates the effect of non-normal incidence P$_2$ and TMI fluxes on the shape of a pyramid with {110} sidewalls. Three of the interfaces between {110} facets are well defined, but the interface in the bottom part of the image is wider due to the formation of a $(2\bar{1}1)$B facet. As the pyramid orientation is tilted, figures 5(a)–(c), this new facet (a $(\bar{2}11)$B facet) switches to the top of the image in figure 5(c). In between these orientations, figure 5(b), both the $(2\bar{1}1)$B and $(\bar{2}11)$B facets are simultaneously observed. If the substrate is rotated 90° in the plane, figure 5(e), the $(\bar{2}11)$B

facet is still observed. The observation of the {211}B facets is a consequence of the non-uniform P$_2$ flux across the pyramid, since for both figures 5(b) and (e) the TMI flux is normal to the surface. The extra facet appears on the side of the pyramid where the P$_2$ flux is the lowest. Given the angle between the substrate normal and the P$_2$ gas injector of 17° in figure 5(b), the P$_2$ flux varies by a factor of 1.55 between the {110} facets facing the injector and those tilted away.

The presence of a {211}B facet and its affect on the shape of the (001) surface has important consequences for the deposition of InAs for QD formation. A group V terminated facet such as the {211}B will undergo rapid P to As exchange upon As exposure, leading to an unwanted source of material for QD formation, and consequently a reduced ability to reproducibly form QDs with desired emission properties. Moreover, the {211}B facets act as nucleation sites for QDs (figure 5(d)), which competes with the growth and positioning of a single QD at the apex of the pyramid. Realizing that the growth depends more critically on the uniformity of the P$_2$ flux than the TMI flux the sample was oriented so that the P$_2$ flux was normal to the surface, figure 5(f). This shows a very uniform pyramid with well-defined intersections between the {110} facets, and a well-defined (001) surface, optimal for use as a template for InAs QD growth.

3.3. Growing an InAs quantum dot on an InP pyramid

As shown in figure 2 changing the initial size of the opening in the SiO$_2$ mask, or the amount of InP deposited, the dimensions of the top (001) facet can be controlled. This provides a perfect template for the growth of InAs QDs. For the placement of a single InAs quantum dot the size of the top facet should be of the order of the size of a typical self-assembled InAs QD grown on InP, which is 20–40 nm in diameter [22]. To grow a QD we switch from the deposition of InP to the deposition of InAs. As in the growth of InP, the incorporation preferentially occurs on the (001) surface with the supply of indium coming from the direct impingement of the indium source on the (001) surface and the diffusion of indium off the other facets. This means that the collection area for indium is far greater than the size of the top facet where it incorporates, resulting in a significant increase in the growth rate of the QD over that for conventional planar growth. This enhancement in the growth rate has to be taken into account, and results in the deposition of a very thin InAs layer for the formation of a single QD. As for the planar growth of InAs QDs on InP the dot forms via the strain driven Stranski–Krastanow growth mode [23, 24] at the pyramid top. An example of a single dot forming at the apex of a pyramid can be seen in [25].

As mentioned earlier, small {111} facets are sometimes formed in the initial stages of the pyramidal growth using square patterns opened in the ⟨100⟩ directions, figure 3(a). These occur because the patterning does not produce perfectly square corners in the SiO$_2$ mask and is emphasized if the patterning is poor, with the extreme case being a circle, as shown in figure 1. The formation of {111} facets has a significant impact when InAs QDs are to be grown on the top (001) surface of the pyramid. The exposure of those InP
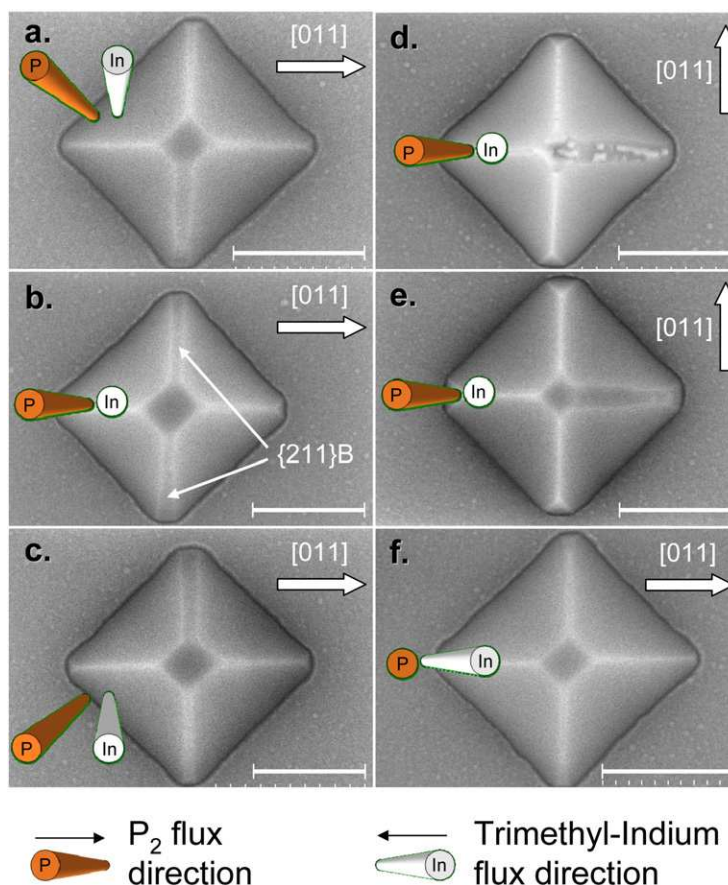
Figure 5. Plan view SEM images of InP pyramid growth without sample rotation and as a function of orientation of the source fluxes (shown schematically). (a)–(c) Growth with progressive tilt of the sample orientation, note that for (b) the TMI flux is normal to the surface. (e) Same orientation of the fluxes to the surface as in (b) but with a sample rotation of 90° about the surface normal. (d) Same orientation as in (e) but with a thin layer of InAs grown on top. InAs quantum dots are seen on the (100) and (21$\bar{1}$)B surfaces. (f) The sample is tilted so that the P_2 flux is normal to the surface. Note that the {211}B facets are no longer present. The arrows indicate the substrate crystal orientation. The scale bar is 300 nm.

(This figure is in colour only in the electronic version)

{111}B facets to an arsenic flux during InAs deposition results in significant quantities of indium being released from the {111}B facets that will then diffuse to the top (001) surface. This makes controlling the quantum dot growth very difficult since the amount of InAs available for dot growth then depends on the size of the {111}B facets. It is thus essential to produce patterns in the SiO_2 mask with square corners, or at least create very well-defined faceting so that this process occurs in the same way for all pyramids. An extreme case of the P to As exchange is demonstrated in figure 6 where the InP pyramid is exposed to an As flux at growth temperature for 5 min before cool down. The regions where the {111}B facets were have been significantly modified with a large quantity of mass transport of indium from these regions to the (001) facet occurring. This excess indium then creates InAs in the form of dots at the top of the pyramid.

A square based pyramid structure is not the only shape that can be successfully grown using a combination of {110} facets with the top (001) surface. The square opening can be stretched into a rectangle which results in a modification of the shape of the (001) surface used as the template for the dot growth. This will then cause a change in the shape of the QD that can be
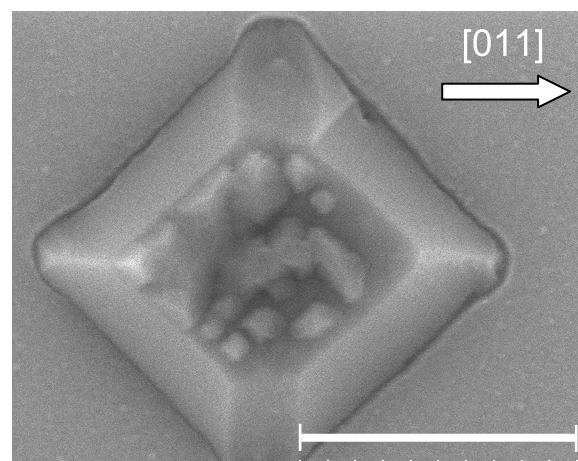

Figure 6. Plan view SEM image of an InP pyramid that has been exposed to an As flux for 5 min at growth temperature before cool down. The scale bar is 500 nm.

grown on that surface. An example of this shape modification is shown in figure 7 where the initial mask opening is changed from square to rectangular. This results in the InAs layer
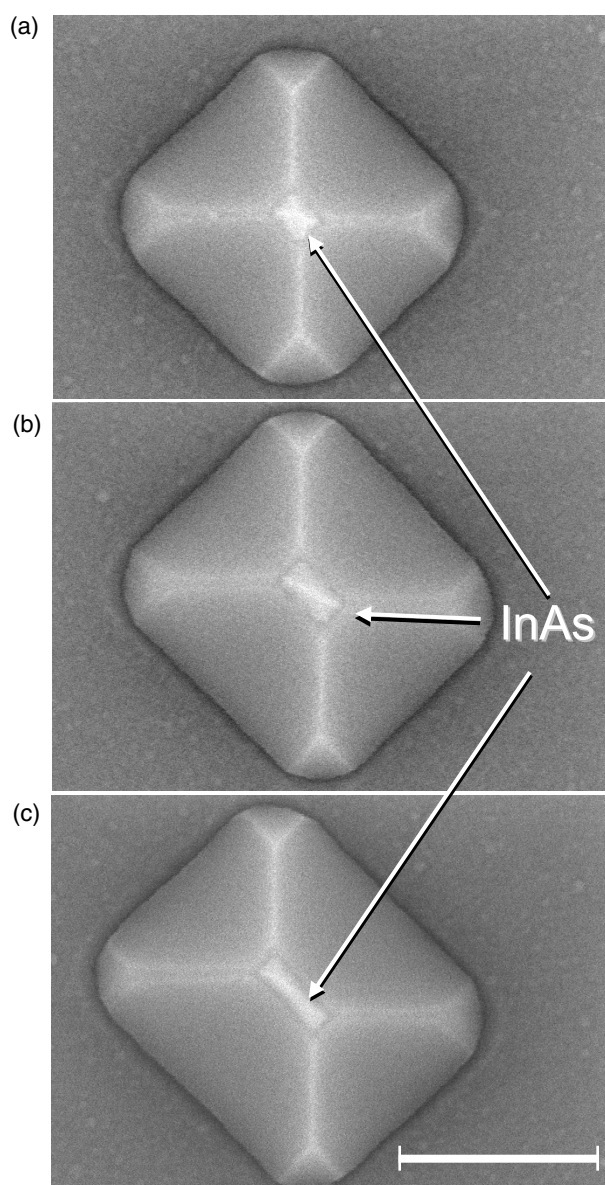
(a)

(b)

(c)

InAs

Figure 7. Plan view SEM images of InP pyramids grown using a square (a), and different rectangular openings (b), and (c) in the SiO$_2$ mask. A thin InAs layer is then deposited on the pyramid. The scale bar is 300 nm.

changing from a square to a wire-like rectangular geometry. This will have a significant impact on the symmetry of the QD states, and demonstrates the ability of the patterned growth to not only control dot position but also affect the symmetry of the electronic structure [25, 26].

3.4. Optical characterization of a single InAs quantum dot

To demonstrate that pyramids and dots can be grown that are not only structurally perfect but also demonstrate high optical quality, photoluminescence (PL) measurements were performed on structures where the InAs QDs were capped with InP. Figure 8 shows a low temperature (4.2 K) PL intensity map of the emission spectra of a single InAs QD in an InP pyramid as a function of laser excitation power. At low
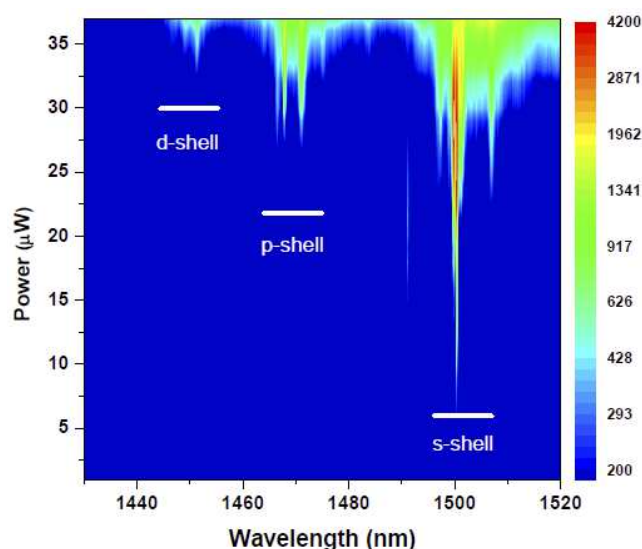

Figure 8. Photoluminescence intensity map of a capped single InAs quantum dot on an InP pyramid as a function of excitation power. Clear s-, p-, and d-shell emission is observed. A ground state linewidth of 50 μeV is measured.

excitation power a single emission line is observed with a linewidth of 50 μeV. With increasing excitation power more lines appear, grouped into s-, p-, and d-shells, as indicated in the figure. This is a general characteristic of the emission from single InAs QDs observed in both the InP and GaAs material systems. The PL shown in figure 8 is directly comparable to that observed for InAs dots grown on conventional planar InP substrates [27], being similar in both intensity and linewidth. This is a direct indication that the pyramidal template is not causing a degradation of the QD quality.

4. Conclusion

In conclusion, nanopyramids with high geometrical and structural quality have been grown and are used to nucleate luminescent InAs QDs. Preferred faceting of InP growth in selective area epitaxy is shown to depend on two key parameters, the shape of the openings in the SiO$_2$ mask and the orientation of the source flux. For the best pyramid growth the patterning in the SiO$_2$ mask must produce corners that are as square as possible, and the P$_2$ flux should be normal to the substrate surface. The quality of dots grown on these optimized pyramids is demonstrated to be very high, equivalent to those grown on more conventional planar structures. The proven ability to control the location of luminescent QDs represents an important milestone in the quest to build nanophotonic devices with increased complexity.

Acknowledgments

References

[1] Santori C, Pelton M, Solomon G, Dale Y and Yamamoto Y 2001 Triggered single photons from a quantum dot *Phys. Rev. Lett.* **86** 1502–5

[2] Michler P, Kiraz A, Becher C, Schoenfeld W V, Petroff P M, Zhang L, Hu E and Imamoglu A 2000 A quantum dot single-photon turnstile device *Science* **290** 2282–5

[3] Stevenson R M, Young R J, Atkinson P, Cooper K, Ritchie D A and Shields A J 2006 A semiconductor source of triggered entangled photon pairs *Nature* **439** 179–82

[4] Shields A J 2007 Semiconductor quantum light sources *Nat. Photon.* **1** 215–23

[5] Kiraz A, Atatüre M and ImamoÄŸlu A 2004 Quantum-dot single-photon sources: prospects for applications in linear optics quantum-information processing *Phys. Rev.* A **69** 032305

[6] Vahala K J 2003 Optical microcavities *Nature* **424** 839–46

[7] Badolato A, Hennessy K, Atature M, Dreiser J, Hu E, Petroff P M and Imamoglu A 2005 Deterministic coupling of single quantum dots to single nanocavity modes *Science* **308** 1158–61

[8] Kapon E, Pelucchi E, Watanabe S, Malko A, Baier M H, Leifer K, Dwir B, Michelini F and Dupertuis M-A 2004 Site- and energy-controlled pyramidal quantum dot heterostructures *Physica* E **25** 288–97

[9] Chithrani D, Williams R L, Lefebvre J, Poole P J and Aers G C 2004 Optical spectroscopy of single, site-selected, InAs/InP self-assembled quantum dots *Appl. Phys. Lett.* **84** 978–80

[10] Reimer M E, Dalacu D, Lapointe J, Poole P J, Kim D, Aers G C, McKinnon W R and Williams R L 2009 Single electron charging in deterministically positioned InAs/InP quantum dots *Appl. Phys. Lett.* **94** 011108

[11] Press D, Gotzinger S, Reitzenstein S, Hofmann C, Loffler A, Kamp M, Forchel A and Yamamoto Y 2007 Photon antibunching from a single quantum-dot-microcavity system in the strong coupling regime *Phys. Rev. Lett.* **98** 117402

[12] Kayser O 1991 Selective growth of InP/GaInAs in LP-MOVPE and MOMBE/CBE *J. Cryst. Growth* **107** 989–98

[13] Amano C, Rudra A, Grunberg P, Carlin J F and Ilegems M 1996 Growth temperature dependence of the interfacet migration in chemical beam epitaxy of InP on nonplanar substrates *J. Cryst. Growth* **164** 321–6

[14] Lobo C and Leon R 1998 InGaAs island shapes and adatom migration behavior on (100), (110), (111), and (311) GaAs surfaces *J. Appl. Phys.* **83** 4168–72

[15] Sugiura H, Nishida T, Iga R, Yamada T and Tamamura T 1992 Facet growth of InP/InGaAs layers on SiO$_2$-masked InP by chemical beam epitaxy *J. Cryst. Growth* **121** 579–86

[16] Matz R, Heinecke H, Baur B, Primig R and Cremer C 1993 Facet growth in selective area epitaxy of InP by MOMBE *J. Cryst. Growth* **127** 230–6

[17] Yamashiki A and Nishinaga T 1999 Arsenic pressure dependence of incorporation diffusion length on (0 0 1) and (1 1 0) surfaces and inter-surface diffusion in MBE of GaAs *J. Cryst. Growth* **198/199** 1125–9

[18] Poole P J, Aers G C, Kam A, Dalacu D, Studenikin S and Williams R L 2008 Selective growth of InP/InGaAs ⟨0 1 0⟩ ridges: physical and optical characterization *J. Cryst. Growth* **310** 1069–74

[19] Poole P J, Lefebvre J and Fraser J 2003 Spatially controlled, nanoparticle-free growth of InP nanowires *Appl. Phys. Lett.* **83** 2055–7

[20] Wong P S, Balakrishnan G, Nuntawong N, Tatebayashi J and Huffaker D L 2007 Controlled InAs quantum dot nucleation on faceted nanopatterned pyramids *Appl. Phys. Lett.* **90** 183103

[21] Kousai S, Yamashiki A, Ogura T and Nishinaga T 1999 Real-time observations of mesa shrinkage process in MBE of GaAs on (1 1 1)B patterned substrates and theoretical analysis *J. Cryst. Growth* **198/199** 1119–24

[22] Robertson M D, Bennett J C, Webb A M, Corbett J M, Raymond S and Poole P J 2005 The determination of the size and shape of buried InAs/InP quantum dots by transmission electron microscopy *Ultramicroscopy* **103** 205–19

[23] Stranski I N and Krastanow L 1938 *Sitz.ber., Akad. Wiss. Math.-Nat.wiss. K1* IIb **146** 797

[24] Leonard D, Krishnamurthy M, Reaves C M, Denbaars S P and Petroff P M 1993 Direct formation of quantum-sized dots from uniform coherent islands of InGaAs on GaAs surfaces *Appl. Phys. Lett.* **63** 3203–5

[25] Kim D, Sheng W, Poole P J, Dalacu D, Lefebvre J, Lapointe J, Reimer M E, Aers G C and Williams R L 2009 Tuning the exciton *g* factor in single InAs/InP quantum dots *Phys. Rev.* B **79** 045310

[26] Kim D *et al* 2005 Photoluminescence of single, site-selected, InAs/InP quantum dots in high magnetic fields *Appl. Phys. Lett.* **87** 212105

[27] Kim D, Lefebvre J, Lapointe J, Reimer M E, Mckee J, Poole P J and Williams R L 2006 Optical spectroscopy of single, planar, self-assembled InAs/InP quantum dots *Phys. Status Solidi* c **3** 3840–3